Cannabidiol enhances the passage of lipid nanocapsules across the blood-brain barrier both *in vitro* and *in vivo*

Juan Aparicio-Blanco [a,b], Ignacio A. Romero [b], David K. Male [b], Karla Slowing [c], Luis García [c], Ana I. Torres-Suárez [a, d,*]

[a] Department of Pharmaceutics and Food Technology, Complutense University, Madrid, Spain

[b] School of Life, Health and Chemical Sciences, Faculty of Science, The Open University, Milton Keynes, United Kingdom

[c] Department of Pharmacology, Pharmacognosy and Botany, Complutense University, Madrid, Spain

[d] University Institute of Industrial Pharmacy, Complutense University, Madrid, Spain

[*]Corresponding author: Prof. Ana I. Torres-Suárez

Department of Pharmaceutics and Food Technology, Complutense University, 28040, Madrid, Spain

Telephone: +34 91 394 1735; e-mail: galaaaa@ucm.es

Abstract

Diseases affecting the central nervous system (CNS) should be regarded as a major health challenge due to the current lack of effective treatments given the hindrance to brain drug delivery imposed by the blood-brain barrier (BBB). Since efficient brain drug delivery should not solely rely on passive targeting, active targeting of nanomedicines into the CNS is being explored.

The present study is devoted to the development of lipid nanocapsules (LNCs) decorated with non-psychotropic cannabinoids as pioneering non-immunogenic brain targeting molecules and to the evaluation of their brain targeting ability both *in vitro* and *in vivo*. Noticeably, both the permeability experiments across the hCMEC/D3 cell-based *in vitro* BBB model and the biodistribution experiments in mice consistently demonstrated that the highest brain targeting ability was achieved with the smallest-sized cannabinoid-decorated LNCs. Importantly, the enhancement in brain targeting achieved with the conjugation of CBD to LNCs outperformed by 6-fold the enhancement observed for the G-Technology® (the main brain active strategy that has already entered clinical trials for the treatment of CNS diseases) As the transport efficiency across the BBB certainly determines the efficacy of the treatments for brain disorders, small cannabinoid-decorated LNCs represent auspicious platforms for the design and development of novel therapies for CNS diseases.

Keywords

Cannabinoids, brain targeting, *in vitro* BBB model, permeability, nanomedicine

1. Introduction

According to the *Mental health: new understanding, new hope* report by the World Health Organization, one in four people will be affected by mental or neurological disorders at some point in their lives, with approximately 450 million people worldwide currently suffering from such conditions. These prevalence data are expected to increase further due to the increase in life expectancy, emphasizing the need to face diseases affecting the central nervous system (CNS) as a major health challenge of the twenty-first century [1]. Unfortunately, the efficacy of the current standard of care for these diseases remains questionable in most cases, since the blood-brain barrier (BBB) truly hinders the distribution to the CNS of most drug substances administered systemically. In consequence, high doses are often required to achieve therapeutically meaningful levels in the CNS, and this causes severe toxicity to peripheral tissues. Therefore, there is a dire need for developing effective strategies of brain drug delivery that overcome biodistribution and pharmacokinetic limitations that account for treatment failure [2-4].

The BBB consists of the endothelial cell monolayer of the brain capillaries closely associated with pericytes and astrocytes and is physiologically responsible for the maintenance of CNS homeostasis. The key features of the brain endothelium that account for the severe restriction to brain drug delivery are both the lack of fenestrations and the presence of tight intercellular junctions [5]. Some of the described delivery strategies to circumvent the BBB such as the direct intracerebral administration [6] and the artificial disruption of the tight junctions by chemical or physical stimuli [7] involve high risk of neurological damage. Hence, every effort is currently being devoted to achieving efficient transport across the brain endothelium with targeted drug carriers following minimally-invasive intravenous injection.

In this regard, the use of nanocarriers arises as an alternative to enhance the passage across the BBB [8]. Noticeably, given their low toxicity, biocompatibility and biodegradability, the clinical trials launched heretofore for the treatment of brain conditions with nanomedicines mostly evaluate lipid-based nanocarriers [9]. Since one major feature that certainly influences the *in vivo* performance of nanomedicines is particle size, a size-controlled extravasation at the target site based on pathophysiological features has traditionally been sought. Nonetheless, although the paracellular permeability of the brain endothelium is altered in most CNS diseases, the BBB dysfunction is typically only substantial in advanced stages of disease and in the most affected sites [10, 11]. Therefore, efficient brain targeting of nanomedicines should not solely rely on passive targeting. To remedy this shortcoming, brain active targeting is being explored with the purpose of boosting transcellularly the delivery efficiency across the BBB [12].

Brain active targeting is based on the modification of nanocarriers with moieties capable of triggering receptor-mediated transcytosis into the CNS through specific binding with endogenous transporters overexpressed on the brain endothelium. Remarkably, the transcytotic mechanisms that mediate the internalization of nanocarriers often follow a size-dependent pattern within the range 10-100 nm. In these cases, a fine control on particle size will certainly improve their potential therapeutic

outcome. Various receptors highly expressed on the cerebral endothelial cells (such as transferrin receptor [13, 14], nicotinic acetylcholine receptor [15, 16], low-density lipoprotein receptor [17, 18] and glucose transporter [19, 20]) have been utilized to develop brain active targeting strategies. However, the translational impact of brain active targeting in clinical trials remains modest, as only three out of the eight liposomes that have made their way to clinical trials for distinct brain conditions following intravenous administration are actively-targeted (ClinicalTrials.gov identifiers: NCT01386580, NCT02048358 and NCT02340156). This is greatly due to the flaws that currently available targeting moieties have: on the one hand, the use of physiological ligands as targeting moieties can develop competitive phenomena with their endogenous counterparts and consequently alter brain homeostasis; whereas on the other hand, the use of targeting peptides must ensure non-immunogenicity [12]. Hence, novel brain targeting moieties are strongly needed.

Since any ligand for which a receptor exists on the cerebral endothelial cells may be potentially used for brain targeting, research on innovative exogenous non-immunogenic ligands are likely to thrive in the near future. In this regard, we hypothesized that cannabinoids hold great promise for brain active targeting. In particular, cannabidiol (CBD), the main phytocannabinoid devoid of psychotropic effects with high BBB transcytosis efficacy, is the appropriate lead candidate to test the possibilities of this hypothesis. Effectively, this cannabinoid has been postulated to bind to various receptors located on the brain endothelium environment [21], namely the CB_1-receptor [22], the serotonin receptor 5-HT_{1A} [23], the transient potential vanilloid receptor type-1 (TRPV-1) [24], the G protein-coupled receptor 55 (GPR55) [25], the adenosine A_{2A} receptor [26] and the dopamine receptor D2 [27].

Therefore, we decorated lipid nanocapsules (LNCs) with CBD. After having screened the influence of critical parameters of these colloid systems as targeted prolonged release carriers against glioma cells [28], we pioneeringly evaluated herein their brain targeting ability as a first-in-a-new class of exogenous non-immunogenic-targeted carriers for brain active targeting to achieve higher translational impact. The brain targeting ability was evaluated both *in vitro* and *in vivo*. Cell viability, uptake and permeability experiments were conducted on the human brain endothelial cell line hCMEC/D3. The *in vitro* permeability coefficients across the hCMEC/D3 monolayer were validated with *in vivo* data from biodistribution studies in mice. Both the role played by particle size and functionalization with CBD in the extent of passage across the BBB was evaluated.

2. Experimental section

2.1. Materials

Labrafac® lipophile WL 1349 (caprylic-capric acid triglycerides) was kindly supplied by Gattefossé. Kolliphor® HS15 ($C_{18}E_{15}$ polyethylene glycol (15) 12-hydroxystearate) was a gift from BASF. Lipoid® S75 (soybean lecithin with 70% of phosphatidylcholine) was supplied by Lipoid-Gmbh. NaCl was purchased from Panreac. De-ionized water was obtained from a MilliQ® Purification System. The fluorescent dyes 3,3'-dioctadecyloxacarbocyanine perchlorate (DiO) and 1,1′-dioctadecyl-3,3,3′,3′-tetramethylindodicarbocyanine 4-chlorobenzenesulfonate salt (DiD) were purchased

from Invitrogen Molecular Probes. Cannabidiol (CBD) was provided by THC-Pharma. Endothelial Cell Basal Medium-2 (EBM-2) and culture supplements were purchased from Lonza. Dulbecco's Modified Eagle Medium (DMEM) devoid of phenol red was provided by Gibco. Tetramethyl-rhodamine-isothiocyanate–dextran (TRITC-dextran, MW 150 kDa), type I collagen from calf skin, fibronectin from bovine plasma, Hank's Balanced Salt Solution (HBSS), 3-(4,5-dimethyl-2-thiazolyl)-2,5-diphenyl-2H-tetrazolium bromide (MTT), dimethyl-sulfoxide (DMSO) and sterile Nunc Lab-Tek® chamber slides (8 wells, Permanox® slide, 0.8 cm^2/well) were purchased from Sigma-Aldrich. Vectashield® mounting medium with DAPI (H-1200) was provided by Vector Laboratories. Sterile Millicell® Hanging Cell Culture Inserts were supplied by Millipore (12-well culture plates; membrane: polyethylene terephthalate membrane; pore size: 1.0 μm; membrane surface area: 1.1 cm^2).

2.2. Cell line

The human brain endothelial hCMEC/D3 cells were seeded in collagen-coated flasks and cultured in EBM-2 medium supplemented with 2.5% foetal bovine serum (FBS), 0.025% (v/v) rhEGF, 0.025% (v/v) VEGF 0.025% IGF, 0.1% (v/v) rhFGF, 0.1% (v/v) gentamycin, 0.1% (v/v) ascorbic acid and 0.04% (v/v) hydrocortisone at 37ºC in 95% air and 5% CO_2. For all experiments, cells between passage 25 and 30 were used.

2.3. Animals

Male ICR mice, aging 4-5 weeks and weighting 29 $\pm$ 3 g, were purchased from Envigo. The mice were housed in ventilated cages with free water and food in a 12h dark/light cycle. Animals were acclimated for one week before the experiment. All *in vivo* experiments were approved by the Ethics Committee of the Community of Madrid (Ref. PROEX 111/14) and conducted according to Spanish and European guidelines (Directive 86/609/EEC).

2.4. Preparation and characterization of lipid nanocapsules (LNCs)

2.4.1. Blank LNCs (F1, F2)

LNCs were prepared by the phase inversion temperature (PIT) method. This low energy method has recently been fully characterized in [29]. Succinctly, Labrafac® lipophile WL 1349, Kolliphor® HS15, Lipoid® S75, NaCl and water were mixed under magnetic stirring and progressively heated over the phase inversion temperature of the system. Subsequently, the mixture was gradually cooled down until the phase inversion temperature was reached (namely, 70 ºC). Then, a sudden quench with cold water (5 mL) was performed to obtain the final suspension of LNCs. By varying the relative proportions of the excipients as shown in Table 1, blank LNCs in different sizes were prepared.

2.4.2. Fluorescently-labeled LNCs (F3, F4, F5, F6)

The fluorescent dyes DiO and DiD were encapsulated in LNCs for particle tracking purposes in *in vitro* and *in vivo* experiments, respectively. To prepare the dye-loaded LNCs, the fluorescent dye was firstly dissolved in the oily phase that constitutes

the core of the LNCs at a weight ratio of 15 mg of dye/g of Labrafac® lipophile WL1349. Then, the remaining excipients were added and progressively heated and cooled down around the phase inversion temperature as indicated in 2.4.1.

2.4.3. LNCs decorated with cannabidiol (CBD) (F7, F8, F9, F10)

Pre-formed fluorescently-labeled LNCs were incubated with a CBD solution (15 mg/mL) in a 3:1 (v/v) ratio. The mixture was gently stirred overnight (250 rpm) until complete solvent evaporation following a previous protocol for the adsorption of targeting moieties on the surface of LNCs with minor modifications [30]. The contribution of the solvent itself to the size distribution of LNCs was ruled out by incubating LNCs with pure solvent up to above the 3:1 (v/v) ratio.

The detailed excipients weight for each formulation of LNCs is shown in Table 1. The mean volume diameter and polydispersity index (PdI) of each formulation were measured by dynamic light scattering (DLS) using a Microtrac® Zetatrac™ Analyzer (Microtrac Inc., USA). Measurements were done in triplicate.

2.5. *In vitro* cytotoxicity

LNCs were assessed for cytotoxicity against hCMEC/D3 cells using an MTT assay. Briefly, hCMEC/D3 cells were seeded into collagen-coated 96-well plates at a density of 2×10^4 cells/well. After cells had been confluent for 48 hours, they were treated with suspensions of LNCs (200 µL) for 1, 4 and 24 hours in three different experiments. Then, the medium was removed and 60 µL of MTT solution (1 mg/mL) in complete EBM-2 were added to each well and incubated for 4 hours. Afterwards, the media containing MTT was removed and 100 µL of DMSO was added to each well. The plates were agitated for 10 minutes and the absorbance was measured at 570 nm using a microplate reader (FLUOstar Omega, BMG Labtech). Experiments were performed in triplicate at each time-point. hCMEC/D3 cells without treatment served as control. Cell viability of each group was expressed as a percentage relative to that of control.

2.6. *In vitro* cellular uptake

2.6.1 Uptake experiments evaluated by flow cytometry

To quantitatively evaluate the BBB targeting ability of LNCs *in vitro*, hCMEC/D3 cells were seeded into collagen-coated 6-well plates at a density of 3×10^5 cells/well. After cells had been confluent for 48 hours, the culture medium was replaced by DiO-labeled LNCs (F3, F4, F7 and F8 at an equivalent dye concentration of 1.65 µg DiO/mL of suspension) suspended in complete EBM-2 (2 mL) wherewith cells were incubated for 4 and 24 hours in two different experiments. Then, cells were rinsed with HBSS, trypsinized and finally resuspended in 0.3 mL HBSS. The fluorescence intensity of cells treated with fluorescent-LNCs was analyzed with a flow cytometer (FACScalibur, BD Biosciences; λ excitation: 488 nm; λ emission: 530 nm). Experiments were performed in triplicate at each time-point. hCMEC/D3 cells treated with blank LNCs served as control. Cellular uptake of each group was expressed as fold-increase in fluorescence mean relative to that of control after correction for the different amount of dye per individual LNC in each formulation.

2.6.2. Uptake experiments evaluated by laser scanning confocal microscopy

To qualitatively illustrate the BBB targeting ability of LNCs *in vitro*, hCMEC/D3 cells were seeded into collagen- and fibronectin-coated chamber slides at a density of 3 x 10^4 cells/well. After cells had been confluent for 48 hours, the culture medium was replaced by undecorated or CBD-functionalized DiO-labeled LNCs at an equivalent dye concentration of 1.65 µg DiO/mL suspended in complete EBM-2 (0.3 mL) wherewith cells were incubated for 24 hours. Then, cells were rinsed with HBSS and mounted with Vectashield® with DAPI mounting medium. The cells were then observed with a laser scanning confocal microscope (Leica SP5, 405 nm for DAPI, 488 nm for DiO) using LEICA LAS AF software. hCMEC/D3 cells treated with blank LNCs served as control. 3D imaging reconstruction was performed by means of IMARIS software.

2.7. Monolayer integrity in the presence of lipid nanocapsules

An *in vitro* BBB model with the human cerebral endothelial cell line hCMEC/D3 was established. Succinctly, hCMEC/D3 cells were seeded into collagen- and fibronectin-coated 12-well hanging cell culture inserts at confluence and incubated for 72 hours in complete EBM-2. The monolayer integrity was assessed by determining the permeability coefficient across the hCMEC/D3 monolayer of the hydrophilic tracer TRITC-dextran both in the presence and the absence of LNCs. Briefly, 400 µL of a TRITC-dextran solution (2 mg/mL) in DMEM without phenol red supplemented with 0.1% (v/v) FBS were added in the apical chamber of both cell-seeded and non-seeded inserts, whereas 1.2 mL of fresh DMEM without phenol red supplemented with 0.1% (v/v) FBS were added in the receptor chamber. At 2, 4, 6, 8, 12 and 24 hours, 200 µL from the basolateral compartment were sampled and replaced with fresh medium. At 24 hours, the apical compartment was likewise sampled (100 µL). The concentration of TRITC-dextran was determined using a microplate reader (FLUOstar Omega, BMG Labtech, excitation wavelength: 544 nm, emission wavelength: 590 nm). The concentrations at the different time points were used to define a linear region within which the permeability coefficients can be calculated [31]. The apparent permeability coefficients were calculated using Equation 1:

$$P_{app}(^{cm}/_{S}) = -\frac{V_D * V_A}{A * t(V_D + V_A)} \ln\left(1 - \frac{(V_D + V_A)}{V_D} \frac{C_A(t)}{C_D(0)}\right) \text{ (Equation 1)}$$

where $C_D(0)$ is the TRITC-dextran concentration placed in the donor compartment at the beginning of the experiment; $C_D(t)$ and C_A (t) are the sample concentrations after the incubation time has elapsed in the donor and acceptor compartment, respectively; t is the time; A is the surface area of the filter insert, and V_D and V_A are the volume of buffer solution in the donor and acceptor compartment, respectively.

To calculate the effective TRITC-dextran permeability (P_{eff}), the contribution of the insert support to the overall resistance was included as detailed in Equation 2:

$$\frac{1}{A * P_{eff}^{hCMEC/D3\ monolayer}} = \frac{1}{A * P_{app}^{cell+filter}} - \frac{1}{A * P_{app}^{filter}} \text{ (Equation 2)}$$

where A is the surface area of the filter insert, $P_{eff}^{monolayer}$ stands for the effective permeability solely due to the hCMEC/D3 monolayer, $P_{app}^{cell+filter}$ is the apparent

permeability calculated for the cell-seeded inserts and P_{app}^{filter} is the apparent permeability calculated for the filters with no cells. Experiments were done in triplicate.

2.8. Transport of LNCs across the hCMEC/D3 monolayer *in vitro*

After having established the *in vitro* BBB model with hCMEC/D3 cell line as described in 2.7, 400 µL of a suspension of DiO fluorescently-labeled LNCs (F3, F4, F7 and F8 at an equivalent dye concentration of 1.65 µg DiO/mL of suspension) in DMEM without phenol red supplemented with 0.1% (v/v) FBS were added in the apical chamber of both cell-seeded and non-seeded inserts, whereas 1.2 mL of fresh DMEM without phenol red supplemented with 0.1% (v/v) FBS were added in the receptor chamber. At 2, 4, 6, 8, 12 and 24 hours, 200 µL from the basolateral compartment were sampled and replaced with fresh medium. At 24 hours, the apical compartment was also sampled (100 µL). The concentration of DiO was determined using a microplate reader (FLUOstar Omega, BMG Labtech, excitation wavelength: 485 nm, emission wavelength: 520 nm). These concentrations were used to calculate the effective permeability coefficients (P_{eff}) as described in 2.7. Only in those cases wherein less than 90% of the DiO dose was recovered between both apical and basolateral chambers, was Equation 1 replaced by Equation 3 to take the retention factor (R) into account:

$$P_{app}(^{cm}/_{s}) = -\frac{V_D * V_A}{A * t(V_D + V_A)} \ln\left(1 - \frac{(V_D + V_A)}{V_D} \frac{C_A(t)}{(1-R) * C_D(0)}\right) \quad \text{Equation 3}$$

2.9. Biodistribution of LNCs in healthy mice

The tissue biodistribution of LNCs was investigated in healthy mice. The mice (n=4-5 per group) were injected via the tail vein with 150 µL of different DiD-fluorescently-labeled LNCs (F5, F6, F9, F10). Ninety minutes (for all formulations) and four hours (for F5 and F9) after administration, mice were sacrificed, and the brain, liver, spleen, kidneys, lungs, heart and blood were collected and homogenized in ethanol for dye extraction. The concentration of DiD was measured using a microplate reader (Varioskan Flash, Thermo Scientific, excitation wavelength: 644 nm, emission wavelength: 665 nm). Results were expressed as percentage of the injected dose per organ.

2.10. Statistical analysis

All experiments were done at least in triplicate and all data are expressed as mean ± SD. Unpaired Student's t test was used for two-group analysis. Statistical significance was fixed as *: $p<0.05$, **: $p<0.01$, ***: $p<0.001$. All the data were analyzed using the GraphPad Prism 7 software.

3. Results

3.1. Preparation and characterization of lipid nanocapsules

Ten different formulations of LNCs were prepared by the PIT method by varying their relative proportions of excipients as detailed in Table 1. Likewise, the size distribution of all LNC formulations is included in Table 1, both in terms of average volume diameter and polydispersity index. In all cases, monodisperse nanocapsules were obtained within the size range of 20-60 nm. In particular, we obtained highly monodisperse blank LNCs of 20 nm (F1) and 40 nm (F2). Noticeably, the inclusion of

fluorescent dyes did not significantly vary the size distribution of their blank counterparts: after loading F1 and F2 with fluorescent dyes, we obtained analogous 20 nm- (F3 and F5 for DiO and DiD, respectively) and 40 nm- (F4 and F6 for DiO and DiD, respectively) sized LNCs. Conversely, as thoroughly detailed in a previous study[28], the functionalization of LNCs with CBD significantly altered their average volume diameter: the decoration of dye-loaded LNCs with CBD increased the particle size to 40 nm (F7 and F9) and 55 nm (F8 and F10), respectively. This increase in particle size was solely due to the presence of the cannabinoid, since the contribution of the solvent was ruled out following incubation of LNCs with the pure solvent at the same ratio (Figure S1). Hence, the role played by particle size in the BBB targeting properties will be first assessed separately in non-modified LNCs and in CBD-decorated LNCs. As the increase of particle size due to functionalization within this interval (20-60 nm) represents a higher percentage increase than in the most widely explored 100-nm range, should particle size play a statistically significant role in the BBB targeting properties, the influence of CBD-decoration will be then evaluated for equally-sized LNCs to maintain the size variable constant.

Moreover, as thoroughly discussed in a previous article[28], slightly negative zeta potential were obtained for all formulations, although the functionalization strategy with CBD considerably smoothed the zeta potential profiles in comparison to those of unfunctionalized LNCs (namely, a 3.5-3.8-fold reduction in zeta potential profile width), in agreement with the hypothesized superficial location of CBD.

Table 1: Detailed excipients weight and size distribution properties for each formulation of LNC in final suspension.

	F1	F2	F3	F4	F5	F6	F7	F8	F9	F10
Excipient weight (mg)										
Kolliphor® HS15	1934	846	1934	846	1934	846	645	282	645	282
Lipoid® S75	75	75	75	75	75	75	25	25	25	25
NaCl	89	89	89	89	89	89	30	30	30	30
Labrafac® lipophile WL 1349	846	1028	846	1028	846	1028	282	343	282	343
Water	6056	6962	6056	6962	6056	6962	2018	2320	2018	2320
DiO	-	-	12	15	-	-	4	5	-	-
DiD	-	-	-	-	12	15	-	-	4	5
CBD	-	-	-	-	-	-	15	15	15	15

Size distribution										
Average volume diameter (nm)	21.29 ± 0.90	42.50 ± 1.08	22.78 ± 0.49	43.85 ± 0.78	21.11 ± 0.25	40.43 ± 0.65	43.00 ± 2.97	62.75 ± 0.49	38.6 ± 0.96	52.40 ± 0.75
Polydispersity index (PdI)	0.040 ± 0.008	0.052 ± 0.004	0.068 ± 0.016	0.044 ± 0.013	0.037 ± 0.004	0.046 ± 0.03	0.105 ± 0.022	0.083 ± 0.001	0.106 ± 0.007	0.064 ± 0.001

3.2. *In vitro* cytotoxicity

To determine the suitability of LNCs for conducting the *in vitro* experiments with the hCMEC/D3 monolayer, an MTT assay was used. Consistently, hCMEC/D3 cells were incubated with F1 and F2-LNCs at an equivalent concentration of 110 µg of internal oily phase/mL of nanocapsule suspension to ultimately normalize the *in vitro* studies as a function of the different payloads (fluorescent dye). Figure 1 shows the cytotoxicity observed for 1, 4 and 24 hours. Remarkably, no toxicity was observed for none of the LNCs at any time point ($p>0.05$). Therefore, these formulations at this suitable non-toxic concentration (that corresponds to an equivalent concentration of 1.65 µg of DiO/mL for the fluorescently-labeled LNCs) were used hereafter for all subsequent *in vitro* experiments.

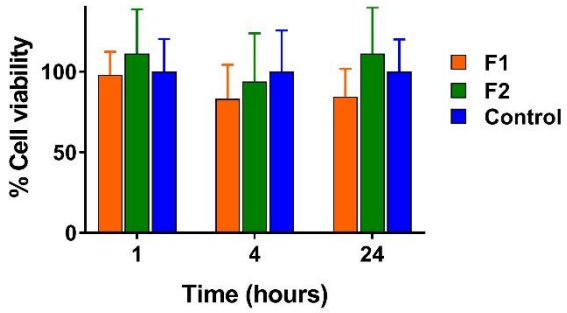

Figure 1: *In vitro* cytotoxicity of LNCs against hCMEC/D3 cells at different time points: 20 nm- (F1) and 40 nm- (F2) sized LNCs in suspension at an equivalent DiO concentration of 1.65 µg DiO/mL ($p>0.05$).

3.3. *In vitro* cellular uptake

The BBB targeting ability of DiO-labeled LNCs (F3, F4, F7 and F8 at an equivalent dye concentration of 1.65 µg DiO/mL of suspension) was tested *in vitro*. The quantitative analysis by flow cytometry of the cellular uptake after 4 and 24 hours of incubation is shown in Figure 2. All formulations exhibited a time-dependent cellular uptake with higher fluorescence intensities after incubating hCMEC/D3 cells with LNCs for 24 hours (**: $p<0.01$). Likewise, a consistent comparison of the role played by particle size can be drawn for non-modified LNCs (F3 vs F4, Figure 2a) and for CBD-decorated LNCs (F7 vs F8, Figure 2b). In both cases the smaller the particle size, the higher their uptake by the human cerebral endothelial cells (***: $p<0.001$ and **: $p<0.01$ at 4 and 24 hours, respectively). Given the influence of particle size in the cellular uptake, the influence of CBD-decoration was then evaluated from a comparison of equally-sized non-modified and CBD-decorated LNCs. Interestingly, the functionalization with CBD

also enhanced the *in vitro* BBB targeting properties of LNC (Figure 2c, ***:p<0.001 and *: p<0.05 at 4 and 24 hours, respectively). The trends in cellular uptake were steady throughout the period evaluated.

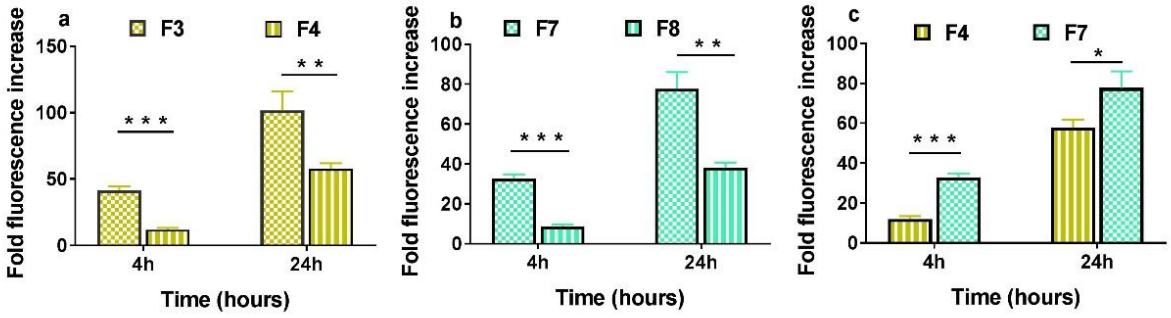

Figure 2: Evaluation of the *in vitro* cellular uptake of LNCs by flow cytometry expressed as folds increase in mean fluorescence intensity versus control. (a) Evaluation of the role of particle size in the *in vitro* cellular uptake (non-modified LNCs) at 4 and 24 hours (***: p<0.001 and **: p<0.01, respectively). (b) Evaluation of the role of particle size in the *in vitro* cellular uptake (CBD-decorated LNCs) at 4 and 24 hours (***: p<0.001 and **: p<0.01, respectively). (c) Evaluation of the role of cannabinoids on the *in vitro* cellular uptake (equally-sized LNCs) at 4 and 24 hours (***: p<0.001 and *: p<0.05, respectively).

The *in vitro* BBB targeting ability of LNCs was further evidenced qualitatively by laser scanning confocal microscopy. As shown in Figure 3, both undecorated and CBD-functionalized LNCs were internalized by hCMEC/D3 in accordance with the data obtained by flow cytometry. The 3D video reconstruction performed by means of the IMARIS software with the Z-stack projections helped evidence that the fluorescent signal from LNCs localized in the intracellular compartment of the cerebral endothelial cells, preferentially in the perinuclear region (Supplementary material).

Given the negligible basal fluorescence of the lipophilic carbocyanine dye in aqueous media as declared by supplier and the lack of release of indocarbocyanine dyes from LNCs even against lipophilic compartments[32] and the lack of detectable transfer of indocarbocyanine fluorescent dyes from LNCs to cells[33], the measured fluorescence is in all cases due to LNC-encapsulated DiO.

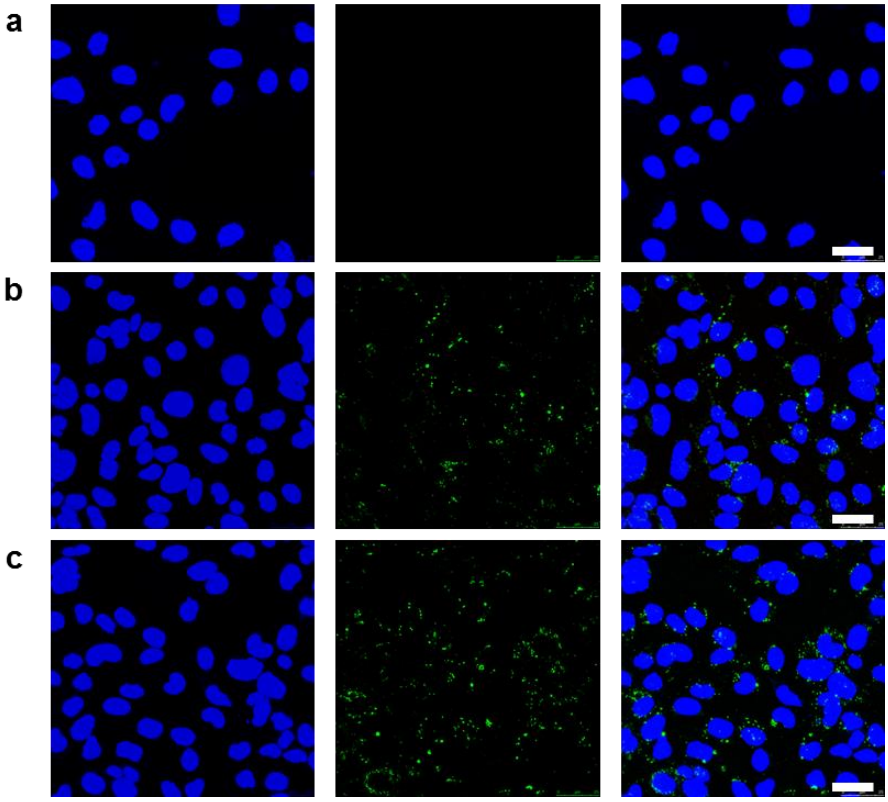

Figure 3: Evaluation of the *in vitro* cellular uptake of LNCs by confocal microscopy: DAPI (left), DiO (center), merged (right). (a) Blank LNCs (F2). (b) DiO-labeled LNCs (F4). (c) CBD-decorated DiO-labeled LNCs (F8). Scale bar = 25 µm. 3D video reconstructions from the Z-stack projections are available as Supplementary material.

3.4. Monolayer integrity of the *in vitro* BBB model in the presence of LNCs

The *in vitro* BBB model with a monolayer of hCMEC/D3 cells was established. This method and the culture conditions had been previously optimized to achieve the highest transendothelial electrical resistance (TEER) value in monoculture [34]. The effect of LNCs on the integrity of confluent cerebral endothelial cell monolayers was investigated by determining the permeability coefficient of fluorescent TRITC-dextran. The cellular model provided permeability coefficients for dextran in the order to those reported in the literature.[35] Importantly, there were no statistically significant differences between the calculated permeability coefficients of TRITC-dextran in the presence and the absence of LNCs ($1.67 \pm 0.44 \times 10^{-7}$ cm/s versus $1.77 \pm 0.33 \times 10^{-7}$ cm/s, $p>0.05$). This restriction to the paracellular route was maintained throughout the assay, confirming that the sample itself did not enhance the paracellular route. Consequently, it was concluded that, during the period evaluated, LNCs did not significantly alter the tightness of the hCMEC/D3 monolayer. These results ultimately enabled the paracellular contribution to the ensuing *in vitro* transport experiments of LNCs across the monolayer to be ruled out during at least 24 hours.

3.5. Transport of LNCs across the hCMEC/D3 monolayer *in vitro*

The BBB transcytosis ability of DiO-labeled LNCs (F3, F4, F7 and F8 at an equivalent dye concentration of 1.65 µg DiO/mL of suspension) was quantitatively assessed *in vitro* by determining the permeability coefficient of LNCs across the hCMEC/D3 monolayer. In line with the results obtained for cellular uptake, a consistent comparison of the role played by particle size can be drawn for non-modified LNCs (F3 vs F4, Figure 4a) and for CBD-decorated LNCs (F7 vs F8, Figure 4b). In both cases the smaller the particle size, the higher the permeability coefficient and the ensuing BBB transcytosis ability ($6.54 \pm 0.75 \times 10^{-8}$ cm/s versus $2.66 \pm 1.05 \times 10^{-8}$ cm/s, **: $p<0.01$; and $1.15 \pm 0.13 \times 10^{-7}$ cm/s versus $4.63 \pm 0.34 \times 10^{-8}$ cm/s, ***: $p<0.001$, respectively). Given the influence of particle size in the permeability coefficient, the influence of CBD-decoration was then evaluated from a comparison of the permeability coefficients of equally-sized non-modified and CBD-decorated LNCs. Noticeably, as expected from the cellular uptake results, the modification with CBD also enhanced the permeability coefficients of LNCs (Figure 4c, $2.66 \pm 1.05 \times 10^{-8}$ cm/s versus $1.15 \pm 0.13 \times 10^{-7}$ cm/s, ***: $p<0.001$).

As demonstrated in our previous study[28], the slow CBD release from LNCs in cell culture (slower than the timeframes evaluated in the current study) serves to rule out the contribution of the effect of free CBD.

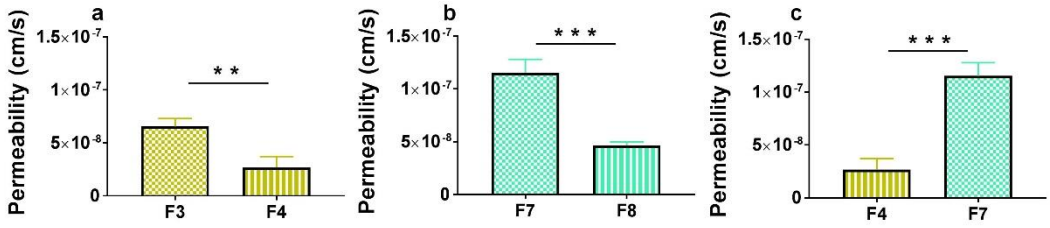

Figure 4: Evaluation of the influence of different factors on the *in vitro* permeability of LNCs across the hCMEC/D3 monolayer. (a) Influence of particle size on permeability coefficients (non-modified LNCs) (**: $p<0.01$). (b) Influence of particle size on permeability coefficients (CBD-decorated LNCs) (***: $p<0.001$). (c) Influence of the modification with CBD on permeability coefficients (equally-sized LNCs) (***: $p<0.001$).

3.6. Biodistribution of LNCs in healthy mice

The BBB targeting properties of DiD-labeled LNCs (F5, F6, F9, F10) were assessed *in vivo*. We ruled out the possible toxicity of our formulations as, on the one hand, for biodistribution experiments in mice, we used the same doses previously reported in the literature as non-toxic for lipid nanocapsules administered intravenously [36] and, on the other hand, cannabidiol has been reported to be tolerated at a dose up to 120 mg/kg in mice (a much higher dose than that one used in the current study)[37, 38]. A proof-of-concept study confirmed that these doses were well tolerated by mice for any of the different tested evaluated in the current study.

For *in vivo* experiments, we switched to the near-infrared dye DiD as it is excited and emits within the wavelength window of 640−800 nm (namely, the wavelength range with the lowest absorption in tissue). We determined the percentage of the injected dose of the different DiD-labeled LNCs located in each major organ (namely, blood, brain,

lungs, kidneys, heart, spleen and liver) following intravenous injection. The blood was estimated to represent 6% of the mice weight to calculate the total percentage of the dose existing in this compartment. The percentages of injected dose in all organs but for the brain are shown in Figure 5. Particle size certainly influences the *in vivo* biodistribution of LNCs: smaller nanocapsules achieved significantly higher plasma levels; whereas bigger LNCs were recognized to a higher extent by the reticuloendothelial organs (liver and spleen). These size-dependent results were consistently obtained both with non-modified LNCs (Figure 5a) and with CBD-decorated LNCs (Figure 5b). Alternatively, for equally-sized LNCs, the presence of CBD helped extend their plasma levels and concomitantly reduced the extent of removal by the liver (Figure 5c).

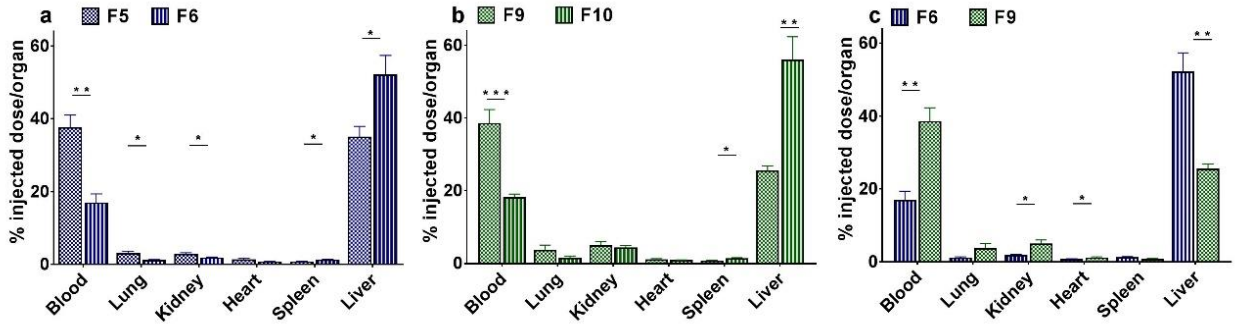

Figure 5: *In vivo* biodistribution of DiD-labeled LNCs in healthy mice 90 minutes after their intravenous injection (expressed as percentage of the injected dose per organ; namely, blood, lungs, kidneys, heart, spleen and liver). (a) Influence of particle size on biodistribution (non-modified LNCs). (b) Influence of particle size on biodistribution (CBD-decorated LNCs). (c) Influence of the modification with CBD on biodistribution (equally-sized LNCs).

The percentage of the injected dose distributed into the brain in each case is shown in Figure 6. In accordance with the *in vitro* results, both particle size and decoration with CBD played a pivotal role in *in vivo* brain targeting. Smaller LNCs showed significantly higher brain targeting properties. This trend was steadily observed both for non-modified LNCs (Figure 6a, 0.185 ± 0.022 % injected dose/brain versus 0.115 ± 0.036 % injected dose/brain, *: $p<0.05$) and for CBD-decorated LNCs (Figure 6b, 0.290 ± 0.088 % injected dose/brain versus 0.116 ± 0.008 % injected dose/brain, **: $p<0.01$). As particle size influenced the extent of brain distribution, the contribution of CBD-decoration was then assessed from a comparison of equally-sized non-modified and CBD-decorated LNCs. Remarkably, the modification of LNCs with CBD significantly contributed to enhance the BBB targeting properties of LNCs *in vivo* (Figure 6c, 0.115 ± 0.036 % injected dose/brain versus 0.290 ± 0.088 % injected dose/brain, *: $p<0.05$).

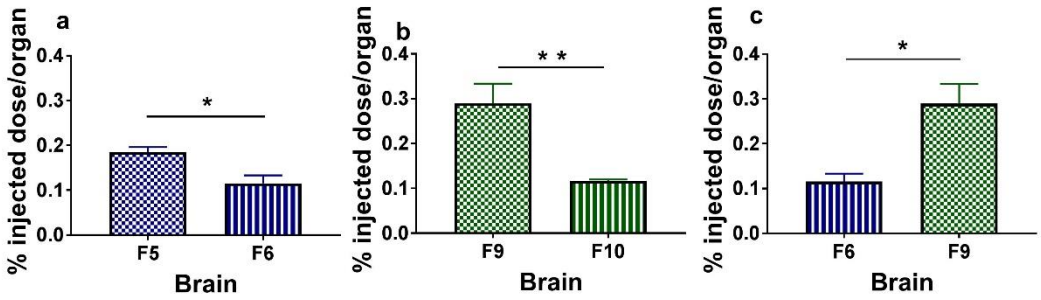

Figure 6: *In vivo* biodistribution of DiD-labeled LNCs in the brain of healthy mice 90 minutes after their intravenous injection (expressed as percentage of the injected dose). (a) Influence of particle size on biodistribution (non-modified LNCs) (*: $p<0.05$). (b) Influence of particle size on biodistribution (CBD-decorated LNCs) (**: $p<0.01$). (c) Influence of the modification with CBD on biodistribution (equally-sized LNCs) (*: $p<0.05$).

The biodistribution of LNCs on a longer term (4 hours after administration) was assessed for those formulations with the highest levels in plasma 90 minutes after administration (namely, F5 and F9). Figures 7 and 8 represent the time-course of the percentage of the injected dose in the major organs and in the brain, respectively. In comparison with their biodistribution at an earlier time point, the percentage of the injected dose in blood and brain decreased with time, whereas the levels in the reticuloendothelial organs progressively augmented. Similar trends were observed for F5 (Figures 7a and 8a) and for F9 (Figures 7b and 8b).

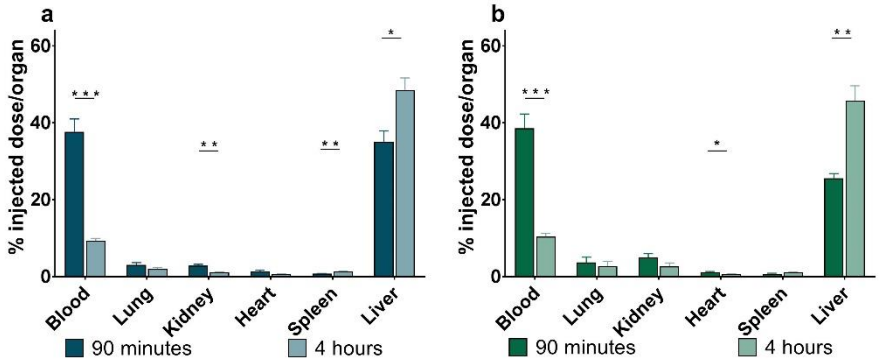

Figure 7: *In vivo* biodistribution of DiD-labeled LNCs in healthy mice (expressed as percentage of the injected dose per organ; namely, blood, lungs, kidneys, heart, spleen and liver). Time-course biodistribution of (a) DiD-labeled LNCs (F5) and (b) CBD-decorated DiD-labeled LNCs (F9).

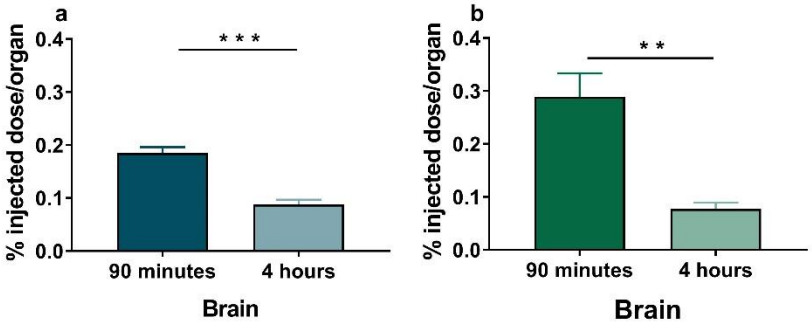

Figure 8: *In vivo* biodistribution of DiD-labeled LNCs in the brain of healthy mice (expressed as percentage of the injected dose). Time-course biodistribution of (a) DiD-labeled LNCs (F5) and (b) CBD-decorated DiD-labeled LNCs (F9).

4. Discussion

Brain diseases represent a major health challenge as brain drug delivery is hampered by the blood-brain barrier (BBB) [39]. To augment the extent of brain drug delivery, intravenously-administered nanomedicines have already reached clinical trials for the treatment of different central nervous system (CNS) diseases (with a focus on brain tumors, but also including neurodegenerative diseases such as multiple sclerosis). Most of these clinical trials evaluate passively-targeted liposomes (ClinicalTrials.gov Identifiers: NCT00734682, NCT02861222, NCT00019630, NCT00944801, NCT01222780). However, given that the hypothesized BBB disruption in most CNS diseases only occurs substantially in advances stages and in the most damaged areas, passive targeting of nanomedicines should be supplemented with brain active targeting [40]. Importantly, for brain active targeting to achieve high translational impact, some criteria in the selection of targeting moieties must be met to prevent competitive phenomena with endogenous substrates and ensure non-immunogenicity [12]. As a result, research on novel exogenous non-immunogenic ligands has become a research hotspot.

In the present study we have prepared cannabidiol (CBD)-decorated lipid nanocapsules (LNCs) as innovative candidates to achieve brain targeting. Their brain targeting ability was evaluated both *in vitro* and *in vivo*. LNCs were chosen according both to their high drug loading potential within their oily core (unlike liposomes) and to their high kinetic stability provided by their solid surfactant shell. These carriers were prepared by the energetically-efficient phase inversion temperature (PIT) method. To evaluate the influence of particle size on the transcytosis mechanisms that mediate brain targeting, monodisperse LNCs in different sizes were prepared by varying the relative proportions of their excipients (Table 1). Alternatively, we hypothesized that given the plethora of receptors of the CNS to which cannabinoids have been reported to bind, cannabinoids hold great promise to enhance the brain targeting properties of nanocarriers. In particular, cannabidiol (CBD), the main cannabinoid devoid of psychotropic effects, seems the appropriate lead candidate to test the possibilities of this hypothesis [21]. Hence, preformed LNCs were decorated with CBD to evaluate its role as brain targeting molecule.

The different LNCs were firstly evaluated *in vitro* with cell viability, uptake and permeability experiments conducted on the human brain endothelial cell line hCMEC/D3. This cell line was used as the *in vitro* BBB model given both their human origin and their better barrier properties in comparison with other commonly used cell lines [41]. Through cell viability experiments on hCMEC/D3 cells. we determined non-toxic concentrations to perform both the uptake and permeability experiments at equivalent concentrations of the dye-labeled LNCs.

The BBB targeting efficiency of dye-labeled LNCs was measured by their cellular uptake through flow cytometry. The internalization of LNCs by hCMEC/D3 followed a time-dependent pattern. Results consistently demonstrated a significantly higher BBB-targeting effect for smaller LNCs (for both unmodified-LNCs and CBD-decorated LNCs) and for CBD-decorated LNCs (for equally-sized LNCs). The images taken by confocal microscopy further evidenced qualitatively the efficient internalization of LNCs. A 3D video reconstruction of the Z-stacks of these images seems to support a perinuclear localization of the LNCs within the hCMEC/D3 cells.

The BBB transcytosis efficiency of dye-labeled LNCs was measured through permeability experiments across the *in vitro* BBB model. The integrity of the BBB model throughout the 24 hours that lasted the permeability experiments was previously demonstrated with TRITC-dextran as hydrophilic tracer: a comparison of the permeability coefficients of TRITC-dextran across the endothelial cell monolayer *in vitro* was not altered by the presence of LNCs ($p>0.05$). As a result, the *in vitro* BBB model was suitable for evaluating the transport ability of the different LNCs. We calculated herein the permeability coefficient as a robust parameter that enables the comparison of the different transport efficiencies. Importantly, permeability coefficient remains constant throughout the experiment, which is not the case for the transport ratio expressed as percentage of passage across the endothelial monolayer. Although this ratio is being broadly utilized to express transport efficiencies [13, 15, 16, 19, 42-45], it varies with the different time points and does not take into account important experimental parameters such as the insert surface area or the volumes of the acceptor and the donor chambers to normalize the data (which is precisely one of the main advantages of *in vitro* studies in comparison with the higher unquantifiable variability of *in vivo* experiments). For this reason, the efficiency of different brain active targeting strategies cannot be readily compared with transport ratios calculated as percentage. In order to attempt a comparison between various BBB-targeting peptides, Chen et al recently evaluated all these ligands in the same nanocarrier [17]. Nevertheless, this strategy will no longer be plausible with the widening of the brain targeting armamentarium. Noticeably, the cellular uptake results were consistent with the permeability experiments: the permeability coefficients across the endothelial monolayer were significantly higher for smaller LNCs (for both unmodified-LNCs and CBD-decorated LNCs) and for CBD-decorated LNCs (for equally-sized LNCs). Taken together, the *in vitro* results highlighted that CBD modification on LNCs plays a major role in the transport enhancement across the BBB model and so does a reduction in particle size (within the tested size-range of 20-60 nm).

The *in vitro* BBB-targeting and penetrating properties across the hCMEC/D3 monolayers were validated with biodistribution studies in mice following intravenous

administration of dye-loaded LNCs. Although brain targeting efficiency has often been evaluated in pathophysiological models, given that BBB dysfunction only occurs in the most damaged brain regions, we aimed at evidencing targeting properties at earlier stages of the CNS diseases with biodistribution studies in healthy mice. Accordingly, we were forced to test smaller-sized nanocapsules (20-55 nm) than the 100 nm-sized (or even above) carriers that have been developed for their evaluation in rodent models of CNS diseases [13, 15, 17, 43, 46, 47].

The *in vivo* results strongly confirmed the promising results obtained with the *in vitro* BBB model as, on the one hand, a decrease in particle size yielded a higher transcytosis rate to brain (1.6-fold increase for unmodified LNCs and 2.5-fold increase for CBD-decorated LNCs) and, on the other hand, the modification of LNCs with CBD showed higher brain targeting properties *in vivo* (2.5-fold increase for equally sized LNCs). The increase in brain levels highly correlated with the higher available plasma concentration and lower recognition by the reticuloendothelial organs observed for these formulations. As also occurred with *in vitro* results, it is often difficult to draw comparisons between *in vivo* results reported by different authors, especially in those studies that only specify the amount of fluorescent tracer distributed into the brain tissue, since this amount depends on the dye dose administered [48-50]. A comparison with those scarce studies that explored the brain targeting properties of carriers within the here tested size range (namely, 20-60 nm) and expressed their results as percentage of the injected dose per gram of brain overall revealed brain levels below those obtained herein [51, 52]. In particular, in [51] the maximal percentage of injected dose per gram of brain tissue (slightly below 0.3% for the targeted nanocarrier) was accomplished at a much later time point (t_{max} around 24h) than the reported herein (0.6% of injected dose per gram of brain tissue at only 90 minutes following intravenous injection). However, it is worth mentioning that all these studies evaluated the biodistribution in glioma-bearing rodent models. Hence, whereas in our study only transcellular routes can be exploited for brain targeting, in the glioma-bearing models the transcellular routes can be significantly supplemented with paracellular pathways across the BBB to enhance the targeting properties (the extent of this contribution will highly depend on the disease stage). As a result, the evaluation of our nanocarrier system in an animal model of disease is expected to exhibit even higher values than those reported herein. Apart from that, Luo et al. had to utilize a double targeting strategy to achieve higher percentage of injected dose per gram of brain tumor [52]. More importantly, enhancement in brain targeting achieved with the conjugation of CBD to LNCs with regard to nude nanocapsules outperformed by 6-fold the enhancement observed for the gluthatione functionalization strategy (around 0.1% of injected dose per gram of brain tissue) assessed in a seminal study with healthy mice that laid the foundations for the G-Technology® (the main brain active strategy that has already entered clinical trials for the treatment of CNS diseases) [53].

Altogether, the enhancement in the brain targeting properties of LNCs achieved with CBD as targeting moiety and with reduction in particle size (within the size range 20-55 nm) has been consistently evidenced both *in vitro* through cellular uptake experiments by flow cytometry and confocal microscopy and through transport

experiments across an endothelial monolayer and *in vivo* through biodistribution studies in healthy mice.

The most likely mechanism of brain targeting of CBD is receptor-mediated transcytosis across the brain endothelium. However, the precise mechanism remains to be experimentally elucidated as the procedure followed for other targeting moieties is not of immediate application in the case of CBD. Targeting residues are often hydrophilic in nature and competitive binding experiments with the free ligand can be conducted *in vitro*. This is not the case for free CBD, where competitive binding experiments would require the inclusion of organic solvents in the culture medium. Moreover, targeting ligands traditionally bind to a single receptor and through a series of experiments conducted in the presence and absence of competitive ligands of those receptors, the extent in the reduction of the targeting ability can be quantified (i.e. transferrin and transferrin receptor). However, CBD has been reported to interact with many different targets [54] and many of those could contribute to the brain active targeting mechanism to different extents (Table 2).

Receptor/Ion channel	Pharmacological role	Ref.
CB_1	Negative allosteric modulator	[22]
CB_2	Negative allosteric modulator	[55]
5-$HT1_A$	Agonist	[23]
TRPV receptors	Agonist	[56]
Glycine receptor	Agonist	[57]
A_{2A}	Agonist	[26]
GPR55	Antagonist	[25]
D_2	Partial agonist	[27]
Nicotinic acethylcholine receptor	Allosteric inhibitor	[58]

Table 2: Overview of the distinct receptors in the CNS environment to which CBD has been postulated to bind. CB_1: cannabinoid receptor type 1, CB_2: cannabinoid receptor type 2, 5-HT_{1A}: serotoninergic receptor, $TRPV_{1–2}$: transient potential vanilloid receptors, A_{2A}: adenosine receptor, GPR55: G-protein-coupled receptor 55, D_2: dopamine receptor.

This fact truly hinders the experimental elucidation of the precise mechanism of brain active targeting of CBD because the precise quantification of the contribution to the BBB-targeting ability of each single receptor through inhibition of the distinct receptors separately is prevented, as inhibiting one receptor recognition may bias the targeting mechanism by upgrading alternative targeting mechanisms. Furthermore, on some of those receptors that CBD binds to, as it is the case of CB_1, CB_2 and nicotinic receptors, CBD acts as an allosteric ligand against which there are no current specific inhibitors available [22, 55, 58].

Further research should be conducted regarding the expression of all these receptors/transporters at the BBB to gain insight into the potential targeting mechanism. So far, of the above mentioned receptors that CBD binds to, at least the nicotinic

acetylcholine receptor and the dopamine receptor have been evidence to be present at the brain endothelium [43, 59] and have started being tested as potential receptors to mediate brain targeting of nanomedicines with exogenous ligands [43, 60]. Therefore, it is assumable that at least these receptors expressed on the cerebral endothelium contribute to the brain active targeting mechanism of CBD across the BBB.

5. Conclusion

We have developed and evaluated pre-clinically both *in vitro* and *in vivo* an innovative BBB-targeted lipid nanocarrier aimed at brain active targeting following intravenous administration. In particular, we obtained monodisperse LNCs by the PIT method and decorated them with non-psychotropic cannabinoids as pioneering brain targeting molecules. Both the permeability experiments across an *in vitro* BBB model and the biodistribution experiments demonstrated that the highest brain transcytosis rate was achieved with the smallest cannabinoid-decorated LNCs. Since the transport efficiency across the BBB certainly determines the efficacy of the treatments for brain disorders, our results indicate that small cannabinoid-decorated LNCs represent a promising platform for the design and development of novel therapies for CNS diseases. Moreover, our study serves to widen with cannabinoids the yet scarce armamentarium of exogenous and non-immunogenic ligands available for brain targeting. Lastly, the consistency between the *in vitro* and *in vivo* results served to validate our *in vitro* BBB model with the human brain endothelial cell line hCMEC/D3 as a versatile screening method to evaluate the passage of nanocarriers across the BBB that meets the high-throughput demands in the early stages of drug discovery and lacks ethical constraints.

Supporting information

Figure on the influence of methanol addition on particle size, 3D video reconstructions of the Z-stack projections imaged by confocal microscopy for the distinct formulations tested (negative control, undecorated and targeted nanocapsules).

Disclosure of interests

The authors declare no competing interests.

Acknowledgements

This work was supported by the Complutense Research Fund (Ref. 16/83) and by the Santander-UCM Research Group Parenteral Administration of Drugs (GR35/10). J. A.-B. would like to thank the Spanish Ministry of Education for his contract within the Professor Training Program FPU (Ref. FPU13/02325) and for funding two research stays at the School of Life, Health and Chemical Sciences, The Open University (Refs. EST15/00534 and EST16/00556). The authors would like to thank to Shereen Nizari for the help provided with the IMARIS software and to Rubén Fernández-de-la-Rosa for the help provided with the intravenous administration to mice.

References

1. Silberberg, D.; Anand, N. P.; Michels, K.; Kalaria, R. N., Brain and other nervous system disorders across the lifespan - global challenges and opportunities. *Nature* **2015,** *527* (7578), S151-S154.

2. Saraiva, C.; Praca, C.; Ferreira, R.; Santos, T.; Ferreira, L.; Bernardino, L., Nanoparticle-mediated brain drug delivery: Overcoming blood-brain barrier to treat neurodegenerative diseases. *J. Control. Release* **2016,** *235*, 34-47.

3. Oberoi, R. K.; Parrish, K. E.; Sio, T. T.; Mittapalli, R. K.; Elmquist, W. F.; Sarkaria, J. N., Strategies to improve delivery of anticancer drugs across the blood-brain barrier to treat glioblastoma. *Neuro-Oncology* **2016,** *18* (1), 27-36.

4. Aparicio-Blanco, J.; Torres-Suarez, A. I., Towards tailored management of malignant brain tumors with nanotheranostics. *Acta Biomater.* **2018,** *73*, 52-63.

5. Abbott, N. J., Blood-brain barrier structure and function and the challenges for CNS drug delivery. *J. Inherit. Metab. Dis.* **2013,** *36* (3), 437-449.

6. Mitragotri, S.; Burke, P. A.; Langer, R., Overcoming the challenges in administering biopharmaceuticals: formulation and delivery strategies. *Nat. Rev. Drug Discov.* **2014,** *13* (9), 655-672.

7. Obermeier, B.; Daneman, R.; Ransohoff, R. M., Development, maintenance and disruption of the blood-brain barrier. *Nat. Med.* **2013,** *19* (12), 1584-1596.

8. Tsou, Y. H.; Zhang, X. Q.; Zhu, H.; Syed, S.; Xu, X. Y., Drug Delivery to the Brain across the Blood-Brain Barrier Using Nanomaterials. *Small* **2017,** *13* (43), 17.

9. Miranda, A.; Blanco-Prieto, M. J.; Sousa, J.; Pais, A.; Vitorino, C., Breaching barriers in glioblastoma. Part II: Targeted drug delivery and lipid nanoparticles. *Int. J. Pharm.* **2017,** *531* (1), 389-410.

10. Sweeney, M. D.; Sagare, A. P.; Zlokovic, B. V., Blood-brain barrier breakdown in Alzheimer disease and other neurodegenerative disorders. *Nature Reviews Neurology* **2018,** *14* (3), 133-150.

11. van Tellingen, O.; Yetkin-Arik, B.; de Gooijer, M. C.; Wesseling, P.; Wurdinger, T.; de Vries, H. E., Overcoming the blood-brain tumor barrier for effective glioblastoma treatment. *Drug Resist. Update* **2015,** *19*, 1-12.

12. Oller-Salvia, B.; Sanchez-Navarro, M.; Giralt, E.; Teixido, M., Blood-brain barrier shuttle peptides: an emerging paradigm for brain delivery. *Chem. Soc. Rev.* **2016,** *45* (17), 4690-4707.

13. Cui, Y.; Zhang, M.; Zeng, F.; Jin, H. Y.; Xu, Q.; Huang, Y. Z., Dual-Targeting Magnetic PLGA Nanoparticles for Codelivery of Paclitaxel and Curcumin for Brain Tumor Therapy. *ACS Appl. Mater. Interfaces* **2016,** *8* (47), 32159-32169.

14. Johnsen, K. B.; Burkhart, A.; Melander, F.; Kempen, P. J.; Vejlebo, J. B.; Siupka, P.; Nielsen, M. S.; Andresen, T. L.; Moos, T., Targeting transferrin receptors at the blood-brain barrier improves the uptake of immunoliposomes and subsequent cargo transport into the brain parenchyma. *Sci Rep* **2017,** *7*, 13.

15. Wei, X. L.; Gao, J.; Zhan, C. Y.; Xie, C.; Chai, Z. L.; Ran, D.; Ying, M.; Zheng, P.; Lu, W. Y., Liposome-based glioma targeted drug delivery enabled by stable peptide ligands. *J. Control. Release* **2015,** *218*, 13-21.

16. Wei, X. L.; Zhan, C. Y.; Shen, Q.; Fu, W.; Xie, C.; Gao, J.; Peng, C. M.; Zheng, P.; Lu, W. Y., A D-Peptide Ligand of Nicotine Acetylcholine Receptors for Brain-Targeted Drug Delivery. *Angew. Chem.-Int. Edit.* **2015,** *54* (10), 3023-3027.

17. Chen, C. T.; Duan, Z. Q.; Yuan, Y.; Li, R. X.; Pang, L.; Liang, J. M.; Xu, X. C.; Wang, J. X., Peptide-22 and Cyclic RGD Functionalized Liposomes for Glioma

Targeting Drug Delivery Overcoming BBB and BBTB. *ACS Appl. Mater. Interfaces* **2017,** *9* (7), 5864-5873.

18. Kim, J. S.; Shin, D. H.; Kim, J. S., Dual-targeting immunoliposomes using angiopep-2 and CD133 antibody for glioblastoma stem cells. *J. Control. Release* **2018,** *269*, 245-257.

19. Byeon, H. J.; Thao, L. Q.; Lee, S.; Min, S. Y.; Lee, E. S.; Shin, B. S.; Choi, H. G.; Youn, Y. S., Doxorubicin-loaded nanoparticles consisted of cationic- and mannose-modified-albumins for dual-targeting in brain tumors. *J. Control. Release* **2016,** *225*, 301-313.

20. Du, D.; Chang, N. D.; Sun, S. L.; Li, M. H.; Yu, H.; Liu, M. F.; Liu, X. Y.; Wang, G. T.; Li, H. C.; Liu, X. P.; Geng, S. L.; Wang, Q.; Peng, H. S., The role of glucose transporters in the distribution of p-aminophenyl-alpha-D-mannopyranoside modified liposomes within mice brain. *J. Control. Release* **2014,** *182*, 99-110.

21. Pisanti, S.; Malfitano, A. M.; Ciaglia, E.; Lamberti, A.; Ranieri, R.; Cuomo, G.; Abate, M.; Faggiana, G.; Proto, M. C.; Fiore, D.; Laezza, C.; Bifulco, M., Cannabidiol: State of the art and new challenges for therapeutic applications. *Pharmacology & therapeutics* **2017,** *175*, 133-150.

22. Laprairie, R. B.; Bagher, A. M.; Kelly, M. E. M.; Denovan-Wright, E. M., Cannabidiol is a negative allosteric modulator of the cannabinoid CB1 receptor. *Br. J. Pharmacol.* **2015,** *172* (20), 4790-4805.

23. Espejo-Porras, F.; Fernandez-Ruiz, J.; Pertwee, R. G.; Mechoulam, R.; Garcia, C., Motor effects of the non-psychotropic phytocannabinoid cannabidiol that are mediated by 5-HT1A receptors. *Neuropharmacology* **2013,** *75*, 155-163.

24. De Petrocellis, L.; Ligresti, A.; Moriello, A. S.; Allara, M.; Bisogno, T.; Petrosino, S.; Stott, C. G.; Di Marzo, V., Effects of cannabinoids and cannabinoid-enriched Cannabis extracts on TRP channels and endocannabinoid metabolic enzymes. *Br. J. Pharmacol.* **2011,** *163* (7), 1479-1494.

25. Ryberg, E.; Larsson, N.; Sjogren, S.; Hjorth, S.; Hermansson, N. O.; Leonova, J.; Elebring, T.; Nilsson, K.; Drmota, T.; Geasley, P. J., The orphan receptor GPR55 is a novel cannabinoid receptor. *Br. J. Pharmacol.* **2007,** *152* (7), 1092-1101.

26. Mecha, M.; Feliu, A.; Inigo, P. M.; Mestre, L.; Carrillo-Salinas, F. J.; Guaza, C., Cannabidiol provides long-lasting protection against the deleterious effects of inflammation in a viral model of multiple sclerosis: A role for A(2A) receptors. *Neurobiol. Dis.* **2013,** *59*, 141-150.

27. Seeman, P., Cannabidiol is a partial agonist at dopamine D2High receptors, predicting its antipsychotic clinical dose. *Transl. Psychiatr.* **2016,** *6*, 4.

28. Aparicio-Blanco, J.; Sebastián, V.; Benoit, J. P.; Torres-Suárez, A. I., Lipid nanocapsules decorated and loaded with cannabidiol as targeted prolonged release carriers for glioma therapy: In vitro screening of critical parameters. *European Journal of Pharmaceutics and Biopharmaceutics* **2019,** *134*, 126-137.

29. Aparicio-Blanco, J.; Sebastián, V.; García-Díaz, H. C.; Rodríguez-Amaro, M.; Torres-Suarez, A. I., Size-tailored design of highly monodisperse lipid nanocapsules for drug delivery. *J. Biomed. Nanotechnol.* **2019,** *15 (in press)*.

30. Carradori, D.; Saulnier, P.; Preat, V.; des Rieux, A.; Eyer, J., NFL-lipid nanocapsules for brain neural stem cell targeting in vitro and in vivo. *J. Control. Release* **2016,** *238*, 253-262.

31. Aparicio-Blanco, J.; Martin-Sabroso, C.; Torres-Suarez, A. I., In vitro screening of nanomedicines through the blood brain barrier: A critical review. *Biomaterials* **2016,** *103*, 229-255.

32. Bastiat, G.; Pritz, C. O.; Roider, C.; Fouchet, F.; Lignieres, E.; Jesacher, A.; Glueckert, R.; Ritsch-Marte, M.; Schrott-Fischer, A.; Saulnier, P.; Benoit, J. P., A new tool to ensure the fluorescent dye labeling stability of nanocarriers: A real challenge for fluorescence imaging. *J. Control. Release* **2013,** *170* (3), 334-342.

33. Simonsson, C.; Bastiat, G.; Pitorre, M.; Klymchenko, A. S.; Bejaud, J.; Mely, Y.; Benoit, J. P., Inter-nanocarrier and nanocarrier-to-cell transfer assays demonstrate the risk of an immediate unloading of dye from labeled lipid nanocapsules. *European Journal of Pharmaceutics and Biopharmaceutics* **2016,** *98*, 47-56.

34. Hatherell, K.; Couraud, P. O.; Romero, I. A.; Weksler, B.; Pilkington, G. J., Development of a three-dimensional, all-human in vitro model of the blood-brain barrier using mono-, co-, and tri-cultivation Transwell models. *J. Neurosci. Methods* **2011,** *199* (2), 223-229.

35. Romero, I. A.; Radewicz, K.; Jubin, E.; Michel, C. C.; Greenwood, J.; Couraud, P. O.; Adamson, P., Changes in cytoskeletal and tight junctional proteins correlate with decreased permeability induced by dexamethasone in cultured rat brain endothelial cells. *Neurosci. Lett.* **2003,** *344* (2), 112-116.

36. Hirsjarvi, S.; Belloche, C.; Hindre, F.; Garcion, E.; Benoit, J. P., Tumour targeting of lipid nanocapsules grafted with cRGD peptides. *European Journal of Pharmaceutics and Biopharmaceutics* **2014,** *87* (1), 152-159.

37. Viudez-Martinez, A.; Garcia-Gutierrez, M. S.; Navarron, C. M.; Morales-Calero, M. I.; Navarrete, F.; Torres-Suarez, A. I.; Manzanares, J., Cannabidiol reduces ethanol consumption, motivation and relapse in mice. *Addict. Biol.* **2018,** *23* (1), 154-164.

38. Deiana, S.; Watanabe, A.; Yamasaki, Y.; Amada, N.; Arthur, M.; Fleming, S.; Woodcock, H.; Dorward, P.; Pigliacampo, B.; Close, S.; Platt, B.; Riedel, G., Plasma and brain pharmacokinetic profile of cannabidiol (CBD), cannabidivarine (CBDV), Delta(9)-tetrahydrocannabivarin (THCV) and cannabigerol (CBG) in rats and mice following oral and intraperitoneal administration and CBD action on obsessive-compulsive behaviour. *Psychopharmacology* **2012,** *219* (3), 859-873.

39. Banks, W. A., From blood-brain barrier to blood-brain interface: new opportunities for CNS drug delivery. *Nat. Rev. Drug Discov.* **2016,** *15* (4), 275-292.

40. Gao, H. L.; Qian, J.; Cao, S. J.; Yang, Z.; Pang, Z. Q.; Pan, S. Q.; Fan, L.; Xi, Z. J.; Jiang, X. G.; Zhang, Q. Z., Precise glioma targeting of and penetration by aptamer and peptide dual-functioned nanoparticles. *Biomaterials* **2012,** *33* (20), 5115-5123.

41. Toman, P.; Lien, C. F.; Ahmad, Z.; Dietrich, S.; Smith, J. R.; An, Q.; Molnar, E.; Pilkington, G. J.; Gorecki, D. C.; Tsibouklis, J.; Barbu, E., Nanoparticles of alkylglyceryl-dextran-graft-poly(lactic acid) for drug delivery to the brain: Preparation and in vitro investigation. *Acta Biomaterialia* **2015,** *23*, 250-262.

42. Jiang, X. Y.; Xin, H. L.; Ren, Q. Y.; Gu, J. J.; Zhu, L. J.; Du, F. Y.; Feng, C. L.; Xie, Y. K.; Sha, X. Y.; Fang, X. L., Nanoparticles of 2-deoxy-D-glucose functionalized poly(ethylene glycol)-co-poly(trimethylene carbonate) for dual-targeted drug delivery in glioma treatment. *Biomaterials* **2014,** *35* (1), 518-529.

43. Belhadj, Z.; Ying, M.; Cao, X.; Hu, X. F.; Zhan, C. Y.; Wei, X. L.; Gao, J.; Wang, X. Y.; Yan, Z. Q.; Lu, W. Y., Design of Y-shaped targeting material for liposome-based multifunctional glioblastoma-targeted drug delivery. *J. Control. Release* **2017,** *255*, 132-141.

44. Su, C. H.; Tsai, C. Y.; Tomanek, B.; Chen, W. Y.; Cheng, F. Y., Evaluation of blood-brain barrier-stealth nanocomposites for in situ glioblastoma theranostics applications. *Nanoscale* **2016,** *8* (15), 7866-7870.

45. Huang, Y. K.; Liu, W. C.; Gao, F.; Fang, X. L.; Chen, Y. Z., c(RGDyK)-decorated Pluronic micelles for enhanced doxorubicin and paclitaxel delivery to brain glioma. *Int. J. Nanomed.* **2016,** *11*, 1629-1641.

46. Gao, J. Q.; Lv, Q.; Li, L. M.; Tang, X. J.; Li, F. Z.; Hu, Y. L.; Han, M., Glioma targeting and blood-brain barrier penetration by dual-targeting doxorubincin liposomes. *Biomaterials* **2013,** *34* (22), 5628-5639.

47. Wei, L.; Guo, X. Y.; Yang, T.; Yu, M. Z.; Chen, D. W.; Wang, J. C., Brain tumor-targeted therapy by systemic delivery of siRNA with Transferrin receptor-mediated core-shell nanoparticles. *Int. J. Pharm.* **2016,** *510* (1), 394-405.

48. Cook, R. L.; Householder, K. T.; Chung, E. P.; Prakapenka, A. V.; DiPerna, D. M.; Sirianni, R. W., A critical evaluation of drug delivery fromligandmodified nanoparticles: Confounding small molecule distribution and efficacy in the central nervous system. *J. Control. Release* **2015,** *220*, 89-97.

49. Wang, B. Y.; Lv, L. Y.; Wang, Z. Y.; Zhao, Y.; Wu, L.; Fang, X. L.; Xu, Q. W.; Xin, H. L., Nanoparticles functionalized with Pep-1 as potential glioma targeting delivery system via interleukin 13 receptor alpha 2-mediated endocytosis. *Biomaterials* **2014,** *35* (22), 5897-5907.

50. Chen, Y. C.; Chiang, C. F.; Chen, L. F.; Liang, P. C.; Hsieh, W. Y.; Lin, W. L., Polymersomes conjugated with des-octanoyl ghrelin and folate as a BBB-penetrating cancer cell-targeting delivery system. *Biomaterials* **2014,** *35* (13), 4066-4081.

51. Luo, Z. M.; Yan, Z. Q.; Jin, K.; Pang, Q.; Jiang, T.; Lu, H.; Liu, X. P.; Pang, Z. Q.; Yu, L.; Jiang, X. G., Precise glioblastoma targeting by AS1411 aptamer-functionalized poly (L-gamma-glutamylglutamine)-paclitaxel nanoconjugates. *J. Colloid Interface Sci.* **2017,** *490*, 783-796.

52. Luo, Z. M.; Jin, K.; Pang, Q.; Shen, S.; Yan, Z. Q.; Jiang, T.; Zhu, X. Y.; Yu, L.; Pang, Z. Q.; Jiang, X. G., On-Demand Drug Release from Dual-Targeting Small Nanoparticles Triggered by High-Intensity Focused Ultrasound Enhanced Glioblastoma-Targeting Therapy. *ACS Appl. Mater. Interfaces* **2017,** *9* (37), 31612-31625.

53. Gaillard, P. J.; Appeldoorn, C. C. M.; Dorland, R.; van Kregten, J.; Manca, F.; Vugts, D. J.; Windhorst, B.; van Dongen, G.; de Vries, H. E.; Maussang, D.; van Tellingen, O., Pharmacokinetics, Brain Delivery, and Efficacy in Brain Tumor-Bearing Mice of Glutathione Pegylated Liposomal Doxorubicin (2B3-101). *PLoS One* **2014,** *9* (1), 10.

54. Bih, C. I.; Chen, T.; Nunn, A. V. W.; Bazelot, M.; Dallas, M.; Whalley, B. J., Molecular Targets of Cannabidiol in Neurological Disorders. *Neurotherapeutics* **2015,** *12* (4), 699-730.

55. Martinez-Pinilla, E.; Varani, K.; Reyes-Resina, I.; Angelats, E.; Vincenzi, F.; Ferreiro-Vera, C.; Oyarzabal, J.; Canela, E. I.; Lanciego, J. L.; Nadal, X.; Navarro, G.; Borea, P. A.; Franco, R., Binding and Signaling Studies Disclose a Potential Allosteric Site for Cannabidiol in Cannabinoid CB2 Receptors. *Front. Pharmacol.* **2017,** *8*, 10.

56. Iannotti, F. A.; Hill, C. L.; Leo, A.; Alhusaini, A.; Soubrane, C.; Mazzarella, E.; Russo, E.; Whalley, B. J.; Di Marzo, V.; Stephens, G. J., Nonpsychotropic Plant Cannabinoids, Cannabidivarin (CBDV) and Cannabidiol (CBD), Activate and Desensitize Transient Receptor Potential Vanilloid 1 (TRPV1) Channels in Vitro: Potential for the Treatment of Neuronal Hyperexcitability. *ACS Chem. Neurosci.* **2014,** *5* (11), 1131-1141.

57. Xiong, W.; Cui, T. X.; Cheng, K. J.; Yang, F.; Chen, S. R.; Willenbring, D.; Guan, Y.; Pan, H. L.; Ren, K.; Xu, Y.; Zhang, L., Cannabinoids suppress inflammatory and neuropathic pain by targeting alpha 3 glycine receptors. *J. Exp. Med.* **2012,** *209* (6), 1121-1134.

58. Mahgoub, M.; Keun-Hang, S. Y.; Sydorenko, V.; Ashoor, A.; Kabbani, N.; Al Kury, L.; Sadek, B.; Howarth, C. F.; Isaev, D.; Galadari, S.; Oz, M., Effects of cannabidiol on the function of alpha(7)-nicotinic acetylcholine receptors. *Eur. J. Pharmacol.* **2013,** *720* (1-3), 310-319.

59. Moura, R. P.; Martins, C.; Pinto, S.; Sousa, F.; Sarmento, B., Blood-brain barrier receptors and transporters: an insight on their function and how to exploit them through nanotechnology. *Expert opinion on drug delivery* **2019**, 1-15.

60. Huey, R.; O'Hagan, B.; McCarron, P.; Hawthorne, S., Targeted drug delivery system to neural cells utilizes the nicotinic acetylcholine receptor. *Int. J. Pharm.* **2017,** *525* (1), 12-20.